RSC Advances

ROYAL SOCIETY OF CHEMISTRY

www.rsc.org/advances

RSC Advances

Mesoporous Carbon/CuS Nanocomposites for pH-dependent Drug Delivery and Near-infrared Chemo-photothermal Therapy

Lei Zhang,[a] Yecheng Li,[b] Zexun Jin,[a] King Ming Chan,[b] and Jimmy C. Yu*[a]

Spurred by the recent development in nanotechnology, multi-functional therapeutic platforms have emerged as promising anti-cancer treatments for their combinational effects. In this paper, we report a novel drug delivery system composing of mesoporous carbon nanospheres (MCN) of 150 to 200 nm in diameter capped with copper sulfide (CuS) nanoparticles (NPs). MCNs can efficiently load doxorubicin (DOX, an anti-cancer drug) due to their hollow and porous structures as well as π-π stacking interactions between MCN and DOX. DOX is retained in MCN at basic and physiological environment, but releases rapidly at acidic environment in its ionized state. Due to the intrinsic near-infrared (NIR) absorption and photothermal conversion ability of copper sulfide nanoparticles, heat is generated for killing tumor cells as well as stimulating DOX release upon NIR irradiation. Thus, this complex (MCN-CuS) exhibits efficient drug loading, low pre-release, temperature-, NIR- and pH-responsive DOX release, and combined antitumor activity.

Introduction

Nanostructures for thermo-chemotherapy have attracted much attention recently, as the combined chemotherapy with hyperthermia results in multi-model interactions and synergistic therapeutic effect.[1] Examples have shown that nanoparticles could overcome multidrug resistance, minimize invasive damage to normal tissues, and improve the anti-cancer efficiency by the synergistic effect.[2-4] Drug delivery vehicles for NIR-triggered release mainly compose of NIR absorption agents and a drug-containing moiety. Noble metal nanoparticles have been used as photothermal therapeutic agents due to their strong light absorption and heat conversion abilities. For example, several studies adopted noble metals supported on the silicon substrate, including silica/Au nanorods,[5] silica/Au nanoshells[6] and silica/Pd nanosheets.[7] In some cases, nanomaterials loading drugs could also act as photothermal ablation agents. Carbonaceous nanomaterials including carbon nanotubes (CNTs) and graphene possess both intrinsic NIR absorption and large drug-loading abilities, with graphene as the representative material. The π-π and hydrophobic interactions between graphene and drugs containing aromatic rings could enhance the loading efficiency.[8, 9] The photothermal effect generated by strong NIR absorption allows graphene-based nanomaterials to be used as NIR-triggered drug carriers [10] and photothermal agents [11].

Effective as these systems are in chemo-photothermal therapy, there are still some limitations. For instance, gold nanoparticles are expensive and suffer from low photo-stability and low photothermal conversion efficiency after laser irradiation.[12] In addition, although carbon-based materials have showed some effective synergistic effect to cancer, they still have relatively low absorption coefficients in the NIR region.[13] Until recently, copper sulfide (CuS), a well-known p-type semiconductor material, has emerged as a new photothermal ablation agent in photothermal therapy. CuS nanoparticles have advantages such as a low cost, low cytotoxicity and intrinsic NIR absorption derived from energy band transitions.[14, 15] Due to its small size and surface area, CuS is rarely directly used as drug delivery vehicles except some reports on CuS nanocages. [16]

To take advantage of CuS nanomaterials, we combine CuS with mesoporous carbon nanospheres (MCNs) for enhancing both drug loading and photothermal conversion efficacy. MCNs are considered to be appropriate carriers for intracellular drug release due to their high surface area, large pore volume and uniform structure. Moreover, specific interactions between MCNs and doxorubicin provide pH-dependent loading (pH ≥ 7.4) and release (pH ≤5.5) properties of DOX from MCNs.[17] Since tumors have lower extracellular pH than normal tissues, and the endosomes and lysosomes possess acidic environments, pH-dependent drug delivery system could reduce the side effects by selective release after their accumulation in tumor sites via the enhanced permeability and retention (EPR) effect.[18]

In this study, MCNs were first synthesized via a hard-template method in hydrothermal conditions. The generated functional groups on the carbon nanospheres endow them both hydrophilicity and intrinsic fluorescence. After removing the template, copper ion and sulfur source were added to

[a] Department of Chemistry, The Chinese University of Hong Kong, Shatin, N.T., Hong Kong SAR, China.
E-mail: jimyu@cuhk.edu.hk; Tel: +852 39436268
[b] School of Life Sciences, The Chinese University of Hong Kong, Shatin, N.T., Hong Kong SAR, China.

MCNs under hydrothermal environment for homogenous growth of CuS on MCN surface. The CuS nanoparticles acted as both gatekeepers from pre-release of payload and photothermal ablation agents for *in vitro* studies. Hence, this nanocomposite (MCN-CuS) exhibited temperature-, NIR- and pH-dependent DOX release, and acted as effective anticancer drug carriers after NIR irradiation as well.

Experimental

Chemicals

Tioacetamide (TAA, $CS(NH_2)_2$) was purchased from Merck. Copper (II) acetate monohydrate ($Cu(CO_2CH_3)_2·H_2O$), cetyltrimethyl ammonium bromide (CTAB), 3-aminopropyltriethoxysilane (APTES), tetramethyl orthosilicate (TMOS) and mesitylene (trimethyl benzene, TMB) were purchased from Sigma-Aldrich (St. Louis, USA). L-(-)-glucose was purchased from Aladdin Reagents (Shanghai, China). All chemicals were of analytical reagent grades and used without further purification.

Spectroscopic and microscopic measurements

The size and morphology of nanoparticles were examined by transmission electron microscopy (TEM) using a Tecnai™ Spirit electron microscope (FEI, Japan). FTIR and UV-vis-NIR absorbance spectra were measured with Nicolet 670 (Thomas Nicolet, USA) and U-3501 (Hitachi, Japan) spectrometer, respectively. The organic content of nanoparticles was measured by thermogravimetric analyzer (TGA) with a heating rate of 10°C/min in a flowing nitrogen atmosphere using TGA6 instrument (Perkin-Elmer, USA). The zeta potentials of the as-synthesized nanoparticles were measured with a commercial zeta-potential spectrometer (ZetaPlus, Brookhaven, USA) with two platinum-coated electrodes and one He–Ne laser as the light source. The hydrodynamic sizes were analyzed with Nanosight NS 500 (Malvern, UK).

Synthesis of MCN and MCN-CuS

First of all, mesoporous silica nanoparticles with ultra large pores (LPMSN) as the template for MCNs were synthesized according to previous report.[19] The mesoporous silica nanoparticles (MSN) were synthesized via a modified Stöber method, with CTAB as the surfactant to generate small pores (~2 nm). To remove CTAB, MSNs were refluxed in ethanol solution containing ~6% HCl overnight, filtered, washed and dried. To prepare LPMSN, as-synthesized MSNs (0.1 g) were dispersed in 10 mL ethanol by sonication for 30min, followed by the addition of 20 mL of 1:1 mixture (v/v) of water and TMB. The mixture was kept at 140 °C in the autoclave for 4 days. The as-synthesized LPMSNs were washed with distilled water and ethanol, and refluxed in in ethanol containing HCl to remove TMB. The prepared LPMSNs (0.1 g) were then suspended in refluxed toluene containing 1 mL of APTES to get amine-functionalized LPMSN (LPMSN-NH₂).

The LPMSNs were coated with carbon layers via hydrothermal method. LPMSN-NH₂ (0.2 g) was first suspended in 15 mL water containing 1.5 g glucose, and sonicated for 30 min before transferring to autoclave. The mixture was kept at 180 °C for 12 h. The thickness of carbon shell could be tuned by the glucose concentration and ratio between nanoparticles and glucose. The carbon coated LPMSN nanoparticles (LPMSN@C) were filtered and dried. The silica core was removed by soaking the nanoparticles in 10% HF solution for 24 h. The as-synthesized MCNs were collected by centrifugation at 14000 rpm for 10 min.

The growth of CuS NPs on MCNs was according to previous report with slight modifications.[20] Typically, 10 mg MCNs were first homogeneously dispersed in 25 mL distilled water by sonication treatment for 2 h, and then 10 mL of 10 mM $Cu(CO_2CH_3)_2·H_2O$ was added. The mixture was stirred at room temperature overnight, followed by addition of 12.5 mL of 16.8 mM NaOH drop by drop. Ten minutes later, the greenish nanoparticles were collected by centrifugation, washed with distilled water twice and suspended with 15 mL of 8 mM TAA. The mixture was transferred to 20 mL Teflon-lined stainless steel autoclave and kept at 160 °C for 4 h. After reaction, the as-synthesized MCN-CuS was washed thoroughly with distilled water and ethanol, and dried in vacuum.

DOX loading and release

MCN and MCN-CuS nanoparticles (10 mg) and DOX (20 mg) were added to PBS buffer (pH=8.5) and stirred for 48 h in darkness at room temperature to reach the equilibrium state. The DOX loaded MCN-CuS was collected by centrifugation and washed with distilled water five times to remove the unloaded DOX. The supernatant containing DOX was all collected and measured with UV-vis spectroscopy to determine the loaded DOX in the carbon nanospheres and nanocomposites. In terms of drug release, certain amounts of MCN and MCN-CuS NPs were suspended in buffers at different pH (4.5 and 7.4). At different time points, the suspension was centrifuged and the DOX concentration in the supernatant was calculated with UV-vis spectrophotometry.

Cell culture, biocompatibility test and the chemo-photothermal therapy *in vitro*

HeLa (human cervical cancer cells), HepG2 (hepatocellular liver carcinoma cells) and C166 (mouse endothelial cells) cells were grown at 37 °C in 5% CO_2 in DMEM supplemented with 10% FBS, 100 units/mL penicillin and 100 μg/mL streptomycin. Both the biocompatibility tests of unloaded nanoparticles and the anticancer effect caused by the photoablation and photothermally controlled DOX release of MCN-CuS were evaluated using Alamar Blue assay. The cells were first seeded onto 96-well plates at a density of $1×10^4$ cells/well and incubated for 24 h. In biocompatibility tests, cells were incubated with different concentrations of MCN and MCN-CuS for 24 h before adding Alamar Blue reagents. In anticancer studies, the cells were exposed to two nanoparticles at 50 μg/mL containing DOX for 3 h, with the same concentration of MCN NPs for comparison. The cells were then irradiated with a 980 nm laser at a power density of 4 W/cm² for 0 to 30 s, followed by incubation for 24 h. The cell medium was replaced with 100 μL fresh medium containing 10% Alamar Blue and incubated for another 2 h. The absorbance was measured at ex 560 nm/em 590 nm using a microplate reader (TECAN Infinite

M200, Switzerland). Experiments were conducted in triplicates and significant differences were analyzed by using PRISM software 6.0.

Confocal laser scanning microscope study

One day before the experiment, 10^5 HeLa cells were seeded in a confocal dish 34.3 mm × 9.3 mm (SPL, Korea). The cells were incubated with MCN and MCN-CuS either with or without DOX (20 µg/mL) at 37°C for 3 h. Staining of acidic organelles were performed according to the manufacturer's protocol (LysoTracker® Red DND-99, ThermoFisher Scientific). Live cell imaging of nanoparticle uptake and DOX release was performed using an Olympus confocal microscope (FV1000 IX81-TIRF) with CO_2 incunator. The intrinsic green fluorescence of MCN and DOX fluorescence were excited at 488 nm and 532 nm. The corresponding emission spectra were 500-530 nm and 560-660 nm, respectively. Images were taken at the same settings before and after NIR irradiation with the 980 nm laser at a power density of 4 W/cm^2 for 30 s. The signal intensity of DOX was compared to calculate the amount of DOX released.

Results and discussion

Synthesis and characterizations of MCN and MCN-CuS.

The anticancer drug-delivery system for photo-chemotherapy was illustrated in Fig. 1a. In this design, we choose mesoporous carbon nanospheres as the loading vehicle due to many advantages. Compared to their counterparts such as carbon nanomaterials or silica mesoporous nanoparticles, MCNs have enhanced surface area and increased pore volume for drug loading.[4, 21] The sp^2 hybridization of the graphitic MCNs makes them favourable for adsorption of electron-rich, aromatic ring-containing molecules. Recently, graphene has been extensively explored as a drug delivery carrier with sheet dimensions of hundreds of nanometers. The two-dimensional structure, however, allows the adsorption of drugs only on the surface. Moreover, the synthesis of graphene with suitable size (sub 100 nm) and approppriate functionalization (for example, the oxidization extent) for biological studies requires strict control.[22] In our study, the template-mediated synthesis method allows strict control in dimension of MCNs by using different templates. Moreover, with the addition of gatekeepers, the pores on MCNs could be blocked to prevent pre-release of drugs, a phenomenon which is usually found in solid carbon nanomaterials. The incorporation of CuS nanoparticles on MCNs enhanced their photothermal conversion ability, especially under irradiation of 980 nm. In previous studies on MCNs for photothermal chemotherapy, people mainly chose 808 nm laser due to the limited absorption ability of MCNs at longer wavelengths.[4, 23, 24] In general, 980 nm laser possesses longer wavelegnth, deeper penetration ability in biological tissues and hence is more suitable for biological studies.[25] Compared to gold nanorod, one of the commonly used NIR-driven photothermal agents, CuS nanoparticles provide us an economical and convenient choice in enhancing photothermal conversion ability. Hence, the combinatin of CuS NPs with MCNs would make a

nanostruture with high drug loading efficiency, NIR-stimulated and pH-dependent drug release properties.

First, large pored-silica nanoparticles (LPMSN) with diameters of 150-200 nm were synthesized from MSN with TMB as the swelling agents to generate ultra large pores for larger surface area and higher loading capacity. After amino-functionalization via the treatment of APTES, the electropositive silica surface could adsorb glucose, due to the electrostatic interactions between the hydroxyl groups (-OH) of the glucose and positively charged ammonium sites.[26]
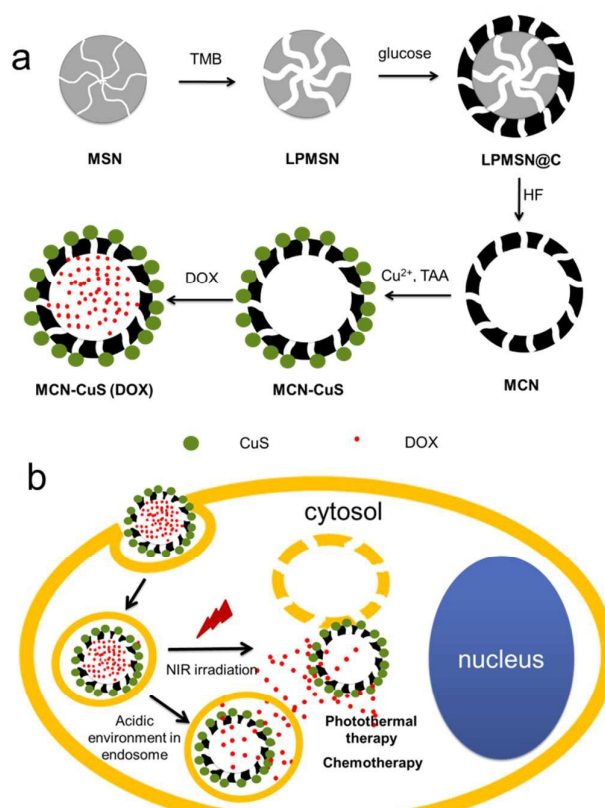

Fig. 1 (a) Schematic illustration of the synthetic process of nanocomposites (MCN-CuS) for chemo-photothermal therapy. (b) Illustration of both pH- and NIR-controlled drug deliveries using DOX loaded MCN-CuS nanocomposites and their application in cancer chemo-photothermal therapy. The acidic environment of endosomes could trigger DOX release from MCN-CuS, and NIR irradiation could cause endocytic disruption, escape of MCN-CuS and DOX release.

These nanospheres (LPMSNs) were used as cores to build a carbon shell on nanoparticles, and then the templates were etched away by hydrofluoric acid (HF). Due to the mesoporous structures of LPMSN, the generated hollow carbon nanospheres also possessed large pores, which could be observed in the TEM images (Fig. 2c). Hydrothermal treatment for CuS growth ensured homogenous capping of CuS nanoparticles on MCNs, as shown in Fig. 2d. The engagement of CuS NPs increased the diameter of MCN to around 200-240 nm. In Fig. 2e, EDX analysis of MCN-CuS nanoparticles confirmed the existance of copper and sulfide on MCN nanoparticles, suggesting successful conjugation of CuS. In

addition, trace amount of silica (atomic 0.92%) showed that almost all the silicon templates have been removed by hydrofluoric acid.
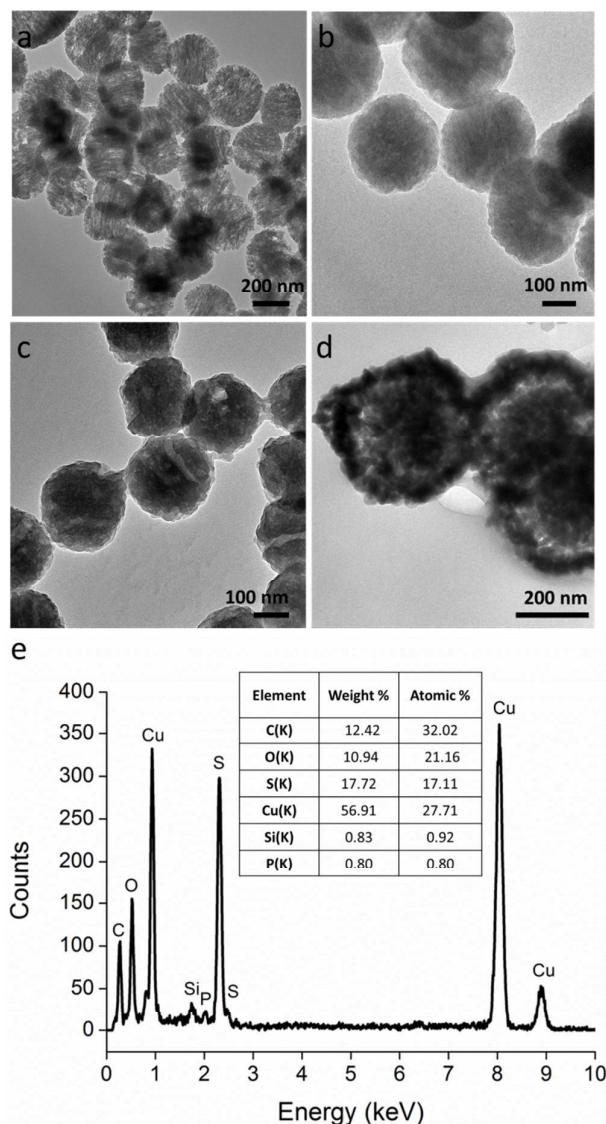

Fig.2 Transmission electron microscopy (TEM) images of (a) LPMSN, (b) LPMSN@C, (c) MCN and (d) MCN-CuS. (e) Qualitative (upper) and quantitative EDX analysis (down) of MCN-CuS nanoparticles confirmed the existence of C, Cu and S, with trace amounts of Si.

During the hydrothermal process of generating carbon layer, the glucose underwent dehydration, condensation or polymerization and aromatization reactions. The generated carbonaceous surface consisted of aromatic structures and reactive oxygen functional groups such as hydroxyl, carbonyl and carboxylic groups,[27] which could be confirmed by the FTIR spectra in Fig.3a. The absorptions at 1701 cm^{-1} and 2923 cm^{-1} could be assigned to C=O and C-H stretching vibrations of aldehyde groups, respectively. The absorption bands at about 1610 and 1510 cm^{-1} could be attributed to C=C stretching

vibrations. The band at 797 cm^{-1} corresponds to aromatic C-H out-of-plane bending vibration, which confirmed the aromatization process during the carbonization. The wide band at around 3390 cm^{-1} was due O-H stretching. In addition, the strong band of LPMSN@C at 1098 cm^{-1} was the skeletal vibration of Si-O network of the MSN core. This band disappeared in MCN and MCN-CuS, suggesting the complete removal of silica core after HF treatment. Intensities of all corresponding peaks in sample MSN-CuS decreased due to the successful coverage of CuS NPs, which could also been observed in TEM image (Fig. 2d).
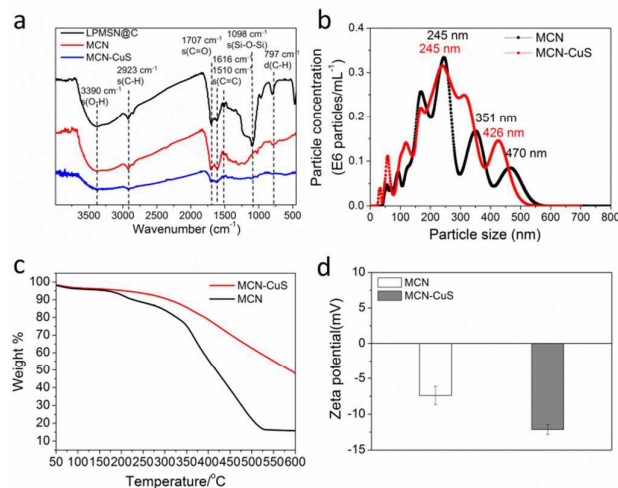

Fig. 3 (a) FTIR spectra of LPMSN@C, MSN and MCN-CuS, (b) hydrodynamic sizes in PBS (pH=7.4) (c) TGA curve and (d) zeta potentials of MCN and MCN-CuS nanoparticles.

Since the carbon-based nanospheres are designed to act as intracellular drug carriers, it is necessary to evaluate their hydrodynamic sizes and zeta potentials to estimate the interactions between nanoparticles and cells. As shown in the distribution of the hydrodynamic sizes (Fig. 3b), the main peaks of MCN and MCN-CuS were 245 nm and 240 nm, which corresponded well with TEM results. However, larger peaks could also be observed in both cases, suggesting partial aggregation of nanoparticles. Although the surfaces of MCN possess hydrophilic functional groups such as carboxylic acid and hydroxyl groups, which could be confirmed by the zeta potential as -7.40 mV (Fig. 3d), they could not form enough electronic repulsion or steric hindrance to prevent nanoparticle aggregation in aqeious conditions. After CuS conjugation on MCN, the zeta potential changed to -12.14 mV, due to the electronegative nature of CuS at neutral environment.[28] In addition, we used thermogravimetric analysis to evaluate the percentage of CuS in MCN-CuS nanocomposites (Fig. 3d). The result indicates the weight percentage of CuS to MCN is about 1:2 in the nanocomposites.

Photothemal heating effect

The prepared nanocomposites exhibited stronger NIR absorption at 980 nm and higher NIR photothermal heating efficiency than pure carbon nanospheres. MCNs did not have absorption at either visible or NIR wavelength, while MSN-CuS

nanocomposites have wide absorption peaks at around 500 nm and 1000 nm (Fig. 4a). The short wavelength absorption agreed with the reported value for the band gap (Eg = 1.85 eV) of bulk CuS. The increased absorption in the NIR region was due to inter-band transitions (absorptions) from valence states to unoccupied states,[29] which suggested the composite as potential photothermal agent. To study the photothermal effect driven by the NIR laser irradiation, the temperature of the solutions containing various concentrations of MCN and MCN-CuS nanocomposites was measured under the irradiation of 980 nm laser (4W/cm^2). As suggested in Fig. 4b, carbon nanospheres did not show obvious photothermal transition efficiency compared to the control (only PBS). However, the MCN-CuS nanocomposites exhibited the ability of quicker and higher temperature elevation. Specifically, the temperature of PBS solution containing 20 µg/mL MCN-CuS (~6.7 µg/mL CuS) rose from 24 °C to 42 °C after irradiation for 240 s, while the one containing 20 µg/mL MCN increased from 24 °C to 39 °C. These properties of nanocomposites suggest the possible application in controllable photothermal therapy.

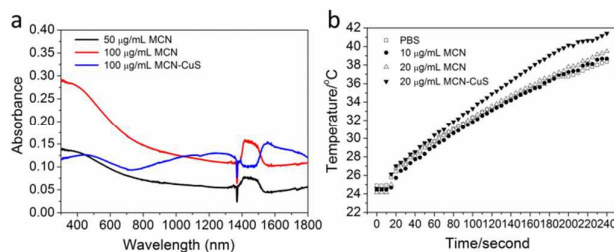**Fig. 4** (a) UV-vis-NIR absorption spectra the 50 µg/mL MCN, 100 µg/mL MCN and 100 µg/mL MCN-CuS nanocomposites. (b) Temperature change of the PBS solution containing the 10 µg/mL MCN, 20 µg/mL MCN and 20 µg/mL MCN-CuS nanocomposites under 980 nm laser irradiation (4W/cm^2), with PBS as control.

DOX loading and release under different stimuli

During DOX loading into MCNs, the initial concentration of DOX in the dispersion was much higher than that inside the MCNs. So DOX would diffuse from the outside to the channels of MSNs driven by the diffusion effect until equilibrium state was reached. DOX is an aromatic anticancer drug and interact with MCNs via π-π stacking as well as hydrophobic interactions. The loading of DOX toward MCN and MCN-CuS was highly pH-dependent, with higher loading capacity in basic solutions (pH>7.4). Due to the ionization of DOX at lower pH values (pKa=8.4),[30] the protonation of NH$_2$ groups of DOX could reduce the hydrophobic interactions between DOX and MCNs and decrease the loading efficiency.[31] So the DOX loading toward MCNs was conducted in basic environment (pH= 8.5) to maximize DOX loading amount. With the method described above, the DOX loading capabilities of MCN and MCN-CuS were calculated to be 220.8 mg/g and 228.7 mg/g, respectively.
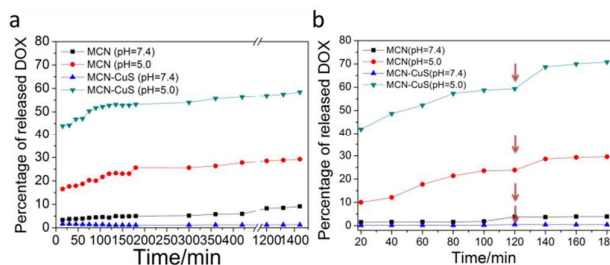

Fig. 5 (a) pH-dependent drug release of DOX and (b) NIR triggered release of DOX at buffers with different pH values from MCN and MCN-CuS nanocomposites with an initial concentration of 2 mg/mL. The NIR irradiation of 980 nm laser (4W/cm^2) was conducted at 120 min for 60s.

As a proof-of concept for the NIR- and pH-dependent DOX release properties, DOX-containing MCN and MCN-CuS were suspended in PBS with different pH values, and the DOX release behavior was recorded (Fig. 5) either with or without irradiation of a 980 nm laser. DOX stacked on both MCN and MCN-CuS remained stable at physiological pH (pH= 7.4), with less than 10% released after about 24 h (Fig 5a). It is obvious that CuS capping could prevent DOX from pre-release, barely with free DOX released from MSN-CuS nanocomposites. In contrast, DOX released immediately after suspending in slightly acidic environment (pH= 5.0), with ~ 25 % and ~ 55% released from MCN and MCN-CuS, respectively. The faster DOX release from MCN-CuS at acidic media may be due to the more hydrophobic property of CuS surface, which was shown in FTIR spectrum of MCN-CuS. Moreover, NIR irradiation would definately enhance the DOX release from MCN and MCN-CuS, with ~5% increase after laser shining at pH 5.0, while the enhancement was barely observable at phsiological pH (Fig. 5b). The combination of different stimuli such as acidic environment and NIR irradiation could bring dramatic increase of DOX release. Hence, both MCN and MCN-CuS nanocomposites could act as controllable pH-sensitive and NIR-stimultated drug carriers with both properties of acid-assisted and NIR-triggered DOX release. In addition, CuS capping could prevent pre-release and increase stimulated drug release. Those properties render MCN-CuS as highly potential drug carriers for anti-cancer treatment. Since nanoparticles are usually internalized into cells via the endocytosis pathway and ended in endosome/lysosomes, the acidic microenvironment of endosome and lysosome (pH= 5-6) could accelerate DOX release and enhance the therapeutic effect.[32]

Biocompatibility of MCN and MCN-CuS

As drug carriers for cancer therapy, the biocompatibility is a substantial prerequisite for *in vitro* and *in vivo* studies. In our study, the cytotoxicity of nanoparticles to HeLa, HepG2 and C166 cells after incubation for 24 h was tested with Alamar Blue assay. C166 is a normal mouse endothelical cell line used to test the cytotoxicity of MCN and MCN-CuS nanoparticles. Since nanoparticles need to cross the endothelical cells of the blood vessels before reaching tumor sites, they are appropriate model cell line for assessing the biocompatibility

of nanoparticles. As shown in Fig. 6, both MCN and MCN-CuS were not obviously toxic to HeLa and HepG2 cells even at the concentration of 100 μg/mL. For C166, MCN and MCN-CuS can actually stimulate cellular growth at higher concentrations (50-100 μg/mL. The low cycotoxcity of CuS nanoparticles was similar to recent report.[33] This suggests the as-synthesized carbon-based nanoparticles are highly compatible to cells and suitable as drug carriers. To minimize the side effects of nanoparticles, the following studies on cellular uptake and anti-cancer effect *in vitro* were done at the nanoparticle concentration smaller than 100 μg/mL.
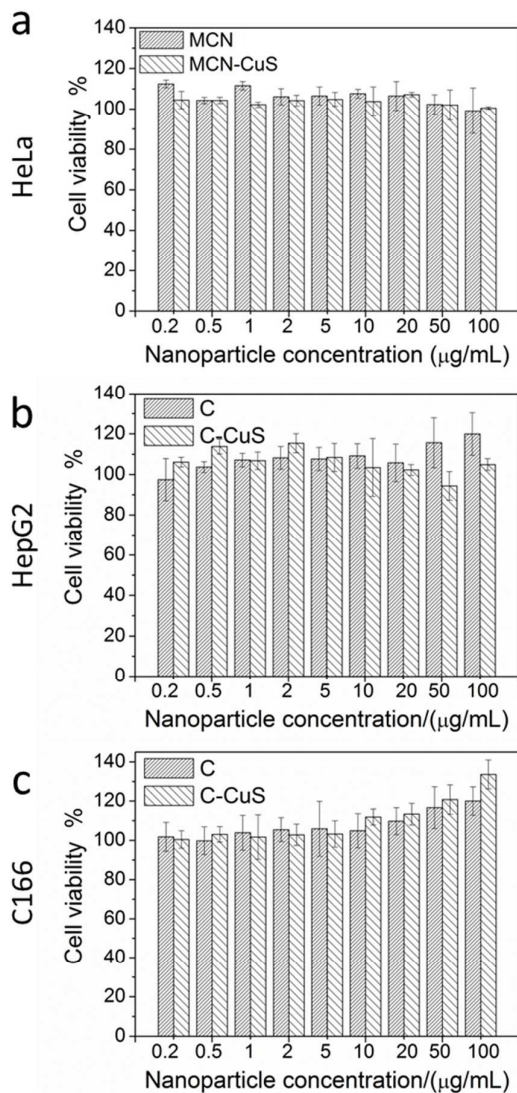

Fig. 6 Alamar Blue assay to assess the cytotoxicity of MCN and MCN-CuS NPs to (a) HeLa (b) HepG2 and (c) C166 cells at different concentrations. Data are means ± S.D. N = 6.

Intracellular fate of MCN and MCN-CuS *in vitro*

Most nanoparticles are known to enter the cells via endocytosis,[34] including some carbon-based materials.[35, 36] In this study, we incubated HeLa cells with MCN and MCN-CuS nanoparticles for 3 h, and then cells were labeled with LysoTracker® Red DND-99 for acidic organelles including lysosomes. Easy tracking the nanoparticles was made possible by intrinsic green fluorescence of MCNs due to functional groups on the surface (Fig. 7).[37] Compared to cells incubated with only DOX, where red signals of DOX could be detected in all cells, both MCN and MCN-CuS were only found in the cytosol and cell surfaces. The overlap of some green signals and black dots (clusters of nanoparticles) in the bright field confirmed the intrinsic green fluorescent property of MCN and MCN-CuS. In addition, the co-localization of the Lysotracker® Red signals and green signals inside the cells confirmed the nanoparticles entered the cells via endocytosis process.
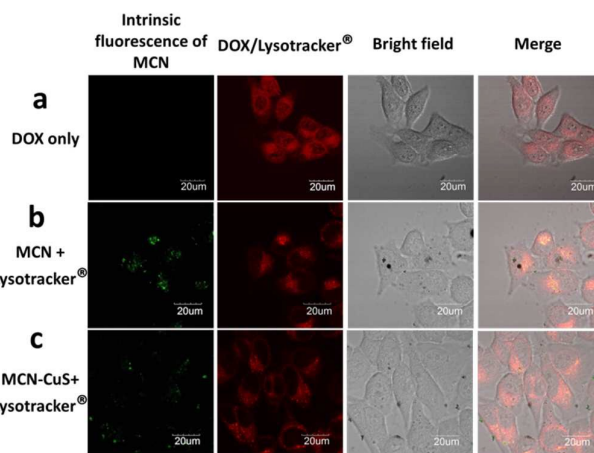

Fig. 7 Confocal images of HeLa cells incubated with (a) 5 μg /mL DOX, (b) 20 μg /mL MCN and (c) 20 μg /mL MCN-CuS for 3 h. Only (b) and (c) were labeled with LysoTracker® Red DND-99 before confocal microscopic studies.

Chemo-photothermal therapy *in vitro*

Cellular uptake of both nanoparticles was performed to explore the effect of NIR irradiation on intracellular DOX release in HeLa cells. After incubation of 20 μg/mL MCN and MCN-CuS for 3 h, excess nanoparticles were completely washed out before NIR irradiation for 30 s. All the confocal images were taken at the same setting for the cells before and after NIR irradiation (Fig. 8). The green-fluorescence of MCNs indicated their intracellular locations. The red fluorescent signal of DOX, on the other hand, could be used to quantify the free DOX released from the carbon nanospheres. Due to the π-π stacked DOX to MCN, the fluorescence decreased significantly after DOX was bound to MCN,[38, 39] while the free DOX exhibited strong red fluorescence intensity. After incubation of nanoparticles for 3 h, both MCN and MCN-CuS nanoparticles have been internalized by the HeLa cells. As suggested by the location of green signals, the nanoparticles were in the cytosol and none were detected in the cell nucleus. Before NIR irradiation, the DOX intensities in both nanoparticles could be detected as partially overlapped with green signals (merged as yellow staining). Some of the free DOX already escaped from the nanoparticles, probably due to the acidic microenvironment of endosome or lysosome, which

is consistent with the cell-free DOX release in acidic environment. After irradiation, the enhanced intensity and enlarged area of DOX signals suggested more free DOX released rapidly. Compared to MCN, MCN-CuS exhibited more DOX release, as indicated by the bright red signal in almost all the cytosol area. The result suggested the MCN-CuS could act as better carriers for NIR-responsive and photothermally enhanced DOX release *in vitro* toward MCN nanoparticles. This result corresponds well with the cell-free DOX release, in which DOX released rapidly from MCN-CuS nanocomposites at acidic environment (Fig. 5).
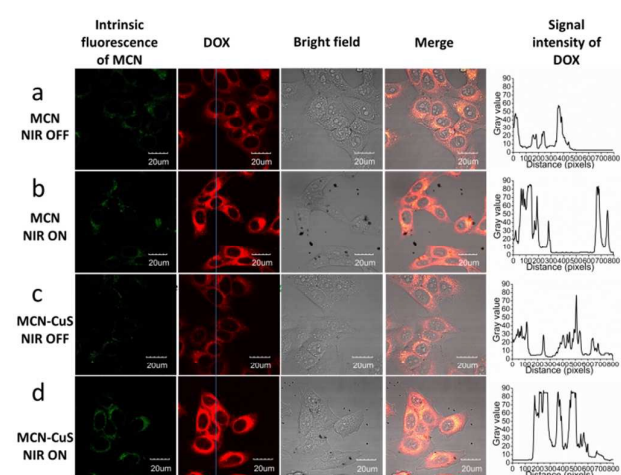

Fig. 8 Confocal images of NIR-responsive DOX release from 20 μg /mL (row a and b) MCN and (row c and d) MCN-CuS in HeLa cells after incubation for 3 h, with the cell images before (row a and c) and after (row b and d) NIR irradiation at a power density of 4 W/cm² for 30s. The histograms assessed the DOX intensities in the blue line were analyzed by software Image J.

Further studies were performed to verify the multi-functional chemo-photothermal therapeutic effects of the nanocomposites *in vitro*. Both HeLa and HepG2 cells were incubated with four groups of nanoparticles (50 μg/mL MCN and MCN-CuS, each with and without DOX) for 3 h, with equivalent DOX added as the fifth group for compasison. After removal of non-internalized nanoparticles and DOX, both cells underwent NIR irradiation (power density 4W/cm²) for different time, with control group as the cells without any treatment. After further incubation for 24 h, the cell viability was tested with Alamar Blue assay. As shown in Fig. 9, the results suggested MCN and MCN-CuS loaded with DOX already showed cytotoxicity to the cancer cells even without irradiation (irradiation time=0s) mianly due to the intracellular release of DOX, while the unloaded MCN and MCN-CuS nanoparticles were not obviously toxic without irradiation. Compared to bare MCN loaded with DOX, MCN-CuS containing DOX had better anti-cancer effect even under no irradiation, which agian was consistent with its quicker DOX release behavior in cell-free PBS (Fig. 5a). Both cells treated with MCN and MCN-CuS nanoparticles under laser irradiation resulted in a decreased cell viability as the irradiation time increased. In all groups with the same irradiation time, DOX-containing MCNs were more toxic than non-loaded ones, suggesting the

chemo-therapy of DOX, for the photothermal effect of sole MCN was not very obvious. In the group under 30s irradiation, cells treated with MCN-CuS nanocomposites, irrespective of DOX, showed the greatest anti-cancer effect, mainly due to the photothermal effect of CuS nanoparticles. Sole DOX treatment to both HeLa and HepG2 cells showed higher cell inhibition than DOX-loaded MCN and MCN-CuS with none and shorter irradiation (0-20s), which could be attributed to partial release of DOX from nanoparticles after 24 h. However, taking its high toxicity into consideration, the incorporation of DOX into drug carriers would prevent its pre-release and reduce its side effects before reaching targeted sites. In addition, it would be impossible to pose on-demand pH- and NIR-triggered release of DOX without drug vechicles. So the CuS capping of MCNs could not only reduce pre-release of DOX, but also greatly enhance the photothermal conversion efficiency and used as photoablation agents for photothermal therapy. The DOX-loading nanocomposites, MCN-CuS, has great promise in applications of chemo-photothermal therapy.
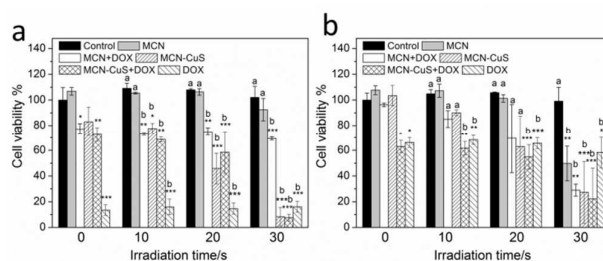

Fig. 9 Alamar Blue assay to assess and the cell viability of (a) HeLa cells, and (b) HepG2 cells incubated with 50 μg/mL MCN and MCN-CuS NPs, then NIR-irradiated for different times. Equivalent DOX was added to the cells and under the same irradiation treatment. Data are means ± S.D. N = 3. Bars with asterisk significant difference from control (*$p < 0.05$, **$p < 0.01$, ***$p < 0.001$; ANOVA, Tukey's test). Bars bearing different lettering are significantly different from group control ($p < 0.05$, ANOVA, Tukey's test).

Conclusions

In summary, a novel nanocomposite design composed of MCN capped with CuS nanoparticles has been developed for high loading of DOX, pH-dependent release and photothermal chemotherapeutic effect. In this platform, the carbon nanospheres lead to large amount loading of hydrophobic drug DOX and pH-dependent DOX release. In addition, functionalized carbon surface makes the nanoparticles intrinsically fluorescent for easy intracellular detection. It is noteworthy that capping of CuS nanoparticles brings irreplacable advantages to MCNs, preventing pre-release of drugs and help accerlerate DOX release under acidic environment. The biocompatible nanostructure guaranteed multifunctional therapeutic effect, with both chemo and photothermal therapy in two cancer cells. This simple and effective drug delivery platform could bring encouraging prospect for cancer therapy and other biomedical applications of MCN.

Acknowledgements

References

1. P. Wust, B. Hildebrandt, G. Sreenivasa, B. Rau, J. Gellermann, H. Riess, R. Felix and P. M. Schlag, *The Lancet Oncology*, 2002, **3**, 487-497.

2. S.-M. Lee, H. Park, J.-W. Choi, Y. N. Park, C.-O. Yun and K.-H. Yoo, *Angewandte Chemie International Edition*, 2011, **50**, 7581-7586.

3. K. Dong, Z. Liu, Z. Li, J. Ren and X. Qu, *Advanced Materials*, 2013, **25**, 4452-4458.

4. Y. Wang, K. Wang, R. Zhang, X. Liu, X. Yan, J. Wang, E. Wagner and R. Huang, *ACS Nano*, 2014, **8**, 7870-7879.

5. B. Hu, L.-P. Zhang, X.-W. Chen and J.-H. Wang, *Nanoscale*, 2013, **5**, 246-252.

6. H. Liu, D. Chen, L. Li, T. Liu, L. Tan, X. Wu and F. Tang, *Angewandte Chemie International Edition*, 2011, **50**, 891-895.

7. W. Fang, S. Tang, P. Liu, X. Fang, J. Gong and N. Zheng, *Small*, 2012, **8**, 3816-3822.

8. Z. Liu, X. Sun, N. Nakayama-Ratchford and H. Dai, *ACS Nano*, 2007, **1**, 50-56.

9. Z. Liu, J. T. Robinson, X. Sun and H. Dai, *Journal of the American Chemical Society*, 2008, **130**, 10876-10877.

10. H. Kim, D. Lee, J. Kim, T.-i. Kim and W. J. Kim, *ACS Nano*, 2013, **7**, 6735-6746.

11. Z. Zhang, J. Wang and C. Chen, *Advanced Materials*, 2013, **25**, 3869-3880.

12. J. Bai, Y. Liu and X. Jiang, *Biomaterials*, 2014, **35**, 5805-5813.

13. Z. M. Markovic, L. M. Harhaji-Trajkovic, B. M. Todorovic-Markovic, D. P. Kepić, K. M. Arsikin, S. P. Jovanović, A. C. Pantovic, M. D. Dramićanin and V. S. Trajkovic, *Biomaterials*, 2011, **32**, 1121-1129.

14. Y. Li, W. Lu, Q. Huang, C. Li and W. Chen, *Nanomedicine*, 2010, **5**, 1161-1171.

15. M. Zhou, R. Zhang, M. Huang, W. Lu, S. Song, M. P. Melancon, M. Tian, D. Liang and C. Li, *Journal of the American Chemical Society*, 2010, **132**, 15351-15358.

16. Y. Wang, Y. Xiao, H. Zhou, W. Chen and R. Tang, *RSC Advances*, 2013, **3**, 23133-23138.

17. J. Zhu, L. Liao, X. Bian, J. Kong, P. Yang and B. Liu, *Small*, 2012, **8**, 2715-2720.

18. V. Torchilin, *Advanced Drug Delivery Reviews*, 2011, **63**, 131-135.

19. M.-H. Kim, H.-K. Na, Y.-K. Kim, S.-R. Ryoo, H. S. Cho, K. E. Lee, H. Jeon, R. Ryoo and D.-H. Min, *ACS Nano*, 2011, **5**, 3568-3576.

20. G. Nie, L. Zhang, X. Lu, X. Bian, W. Sun and C. Wang, *Dalton Transactions*, 2013, **42**, 14006-14013.

21. C. Karavasili, E. P. Amanatiadou, L. Sygellou, D. K. Giasafaki, T. A. Steriotis, G. C. Charalambopoulou, I. S. Vizirianakis and D. G. Fatouros, *Journal of Materials Chemistry B*, 2013, **1**, 3167-3174.

22. M. Skoda, I. Dudek, A. Jarosz and D. Szukiewicz, *Journal of Nanomaterials*, 2014, **2014**, 11.

23. G. Xu, S. Liu, H. Niu, W. Lv and R. a. Wu, *RSC Advances*, 2014, **4**, 33986-33997.

24. H. Wang, Y. Sun, J. Yi, J. Fu, J. Di, A. del Carmen Alonso and S. Zhou, *Biomaterials*, 2015, **53**, 117-126.

25. T. A. Henderson and L. D. Morries, *Neuropsychiatric Disease and Treatment*, 2015, **11**, 2191-2208.

26. Y. Han, X. Dong, C. Zhang and S. Liu, *Journal of Power Sources*, 2012, **211**, 92-96.

27. N. Zhao, S. Wu, C. He, Z. Wang, C. Shi, E. Liu and J. Li, *Carbon*, 2013, **57**, 130-138.

28. M. Nduna, A. E. Lewis and P. Nortier, *Colloids and Surfaces A: Physicochemical and Engineering Aspects*, 2014, **441**, 643-652.

29. K. P. Kalyanikutty, M. Nikhila, U. Maitra and C. N. R. Rao, *Chemical Physics Letters*, 2006, **432**, 190-194.

30. R. J. Sturgeon and S. G. Schulman, *Journal of Pharmaceutical Sciences*, 1977, **66**, 958-961.

31. J. Zhu, L. Liao, X. Bian, J. Kong, P. Yang and B. Liu, *Small*, 2012, **8**, 2715-2720.

32. Z. Liu, A. C. Fan, K. Rakhra, S. Sherlock, A. Goodwin, X. Chen, Q. Yang, D. W. Felsher and H. Dai, *Angewandte Chemie International Edition*, 2009, **48**, 7668-7672.

33. C. Zhang, Y.-Y. Fu, X. Zhang, C. Yu, Y. Zhao and S.-K. Sun, *Dalton Transactions*, 2015, **44**, 13112-13118.

34. T.-G. Iversen, T. Skotland and K. Sandvig, *Nano Today*, 2011, **6**, 176-185.

35. N. Oh and J.-H. Park, *International journal of nanomedicine*, 2014, **9**, 51.

36. H. Jin, D. A. Heller and M. S. Strano, *Nano Letters*, 2008, **8**, 1577-1585.

37. B. R. Selvi, D. Jagadeesan, B. S. Suma, G. Nagashankar, M. Arif, K. Balasubramanyam, M. Eswaramoorthy and T. K. Kundu, *Nano Letters*, 2008, **8**, 3182-3188.

38. Q. Li, B. Sun, I. A. Kinloch, D. Zhi, H. Sirringhaus and A. H. Windle, *Chemistry of Materials*, 2006, **18**, 164-168.

39. N. Nakayama-Ratchford, S. Bangsaruntip, X. Sun, K. Welsher and H. Dai, *Journal of the American Chemical Society*, 2007, **129**, 2448-2449.